Journal of Marine Science and Technology

Volume 25 | Issue 3 Article 9

EXPERIMENTAL STUDY ON HYDRODYNAMIC PERFORMANCE OF A NEW TYPE OF DEEP DRAFT MULTI-COLUMN FDPSO

Jia-Yang Gu
School of Naval Architecture and Marine Engineering, Jiangsu University of Science and Technology, Zhenjiang, China., gujiayang@126.com

Yu-Lin Xie
School of Naval Architecture and Marine Engineering, Jiangsu University of Science and Technology, Zhenjiang, China.

Pei Zhang
School of Naval Architecture and Marine Engineering, Jiangsu University of Science and Technology, Zhenjiang, China.

Yu Chen
School of Naval Architecture and Marine Engineering, Jiangsu University of Science and Technology, Zhenjiang, China.

Xiang-Hong Huang
School of Naval Architecture and Marine Engineering, Jiangsu University of Science and Technology, Zhenjiang, China.

See next page for additional authors

EXPERIMENTAL STUDY ON HYDRODYNAMIC PERFORMANCE OF A NEW TYPE OF DEEP DRAFT MULTI-COLUMN FDPSO

Acknowledgements

This research is financially supported by the National Natural Science Found Project (51309123), the Open Foundation of State Key Laboratory of Ocean Engineering (1407) and the collaborative innovation center funded projects in Jiangsu University (High Technology Ship category).

Authors

Jia-Yang Gu, Yu-Lin Xie, Pei Zhang, Yu Chen, Xiang-Hong Huang, and Yan-Wu Tao

Journal of Marine Science and Technology, Vol. 25, No. 3, pp. 329-342 (2017)
DOI: 10.6119/JMST-017-0215-1

EXPERIMENTAL STUDY ON HYDRODYNAMIC PERFORMANCE OF A NEW TYPE OF DEEP DRAFT MULTI-COLUMN FDPSO

Jia-Yang Gu, Yu-Lin Xie, Pei Zhang, Yu Chen, Xiang-Hong Huang, and Yan-Wu Tao

Key words: multi-column FDPSO, model test, equivalent truncated mooring system, variable cross-section column, spectrum characteristic.

ABSTRACT

This paper presents an experimental study on the hydrodynamic performance of a new type of deep draft multi-column FDPSO. The operating depth of this new type FDPSO is 1500 m. The main dimension, the special variable cross-section column and the cabin arrangement of the octagonal pontoon are introduced. As taking into account the depth limit of the water basin, the 300 m water-depth equivalent truncated mooring system is adopted. The platform's natural period and dimensionless damping coefficient were measured out by the free decay experiment. The FDPSO's motion responses in operation condition and self-survival condition are studied. At the same time, the tension characteristics of mooring system are analyzed. Then, a numerical simulation is adapted to verify the effectiveness of the truncated mooring system. Based on the 3-D potential flow theory, the motion differential equation is calculated by applying the time domain method. The numerical simulation method is also used to study the effect of current velocity on the platform's surge motion response in the self-survival condition. The results of this study would provide references for the design of the variable cross-section column FDPSO.

I. INTRODUCTION

As a new type of integrated ocean platform, floating drilling production, storage and offloading platform (FDPSO) possesses drilling, storage, well completion functions, and has the advantage of maintenance. It can shorten the oil and gas production cycle greatly and reduce investment. As shown in Fig. 1, there are three kinds of structural forms for FDPSO: ship shape, cylinder shape and multi-column shape. American OIL & GAS Company invested the world's first multi-column FDPSO. The main part of this FDPSO is an octagonal floating body with four columns. The maximum operating depth is about 3000 meters.

(a) ship type (b) cylinder type FDPSO (c) multi-column type

Fig. 1. Three typical types of FDPSO.

At present, the deep-water oil and gas developments are still in the early stage, the acquaintance of the oil and gas reservoir condition is not sufficient, so it is necessary to take the trial production for some blocks possessing oil and gas deposits before deciding the development pattern and scale. As relying on the block and without basis construction, the trial production needs to be actualized by synthesizing the functions of drilling, storage and transportation. Hence, the conception of this new type FDPSO is put forward, whose application will greatly cut down the cost of early development of oil fields.

For FDPSO, some researches have been carried out on its conceptual design and mutual coupling hydrodynamic performance between its main-body, mooring system, sheltered riser vessel (SRV) and tension leg deck (TLD). Wang et al. (2013) analyzed the advantages and disadvantages of various FDPSO forms. Taking an octagonal FDPSO as an example, the overall design, optimization design of heave plate and mooring system, hydrodynamic and stability performance were studied.

By combining numerical simulation with model test, Wei et al. (2012; 2014) conducted a research on hydrodynamic performances of ship FDPSO operating in the South China Sea with two kinds of mooring system. The 6-DOF motion responses of FDPSO in operation and self-survival conditions were analyzed. In numerical calculation, the coupling effect between the ship and the anchor was considered. In the basin of State Key Labo-

Paper submitted 07/19/16; revised 10/24/16; accepted 02/14/17. *Author for correspondence: Jia-Yang Gu (e-mail: gujiayang@126.com).*
School of Naval Architecture and Marine Engineering, Jiangsu University of Science and Technology, Zhenjiang, China.

ratory in Shanghai Jiao Tong University, the static water free decay test, white noise test and irregular wave test were carried out successively. Through comparing the results of numerical calculation and the model test, the reliability of the numerical calculation method was verified.

By using SESAM software, Korbijn et al. (2005) studied the dynamic responses and mooring characteristics of an octagonal FDPSO in frequency domain and time domain, and the experiment was carried out in the basin of St Petersburg Ship Scientific Research Center of Russia. Based on the researches on the platform motion responses, the vortex induced motion characteristics of FDPSO were studied, and the maritime transport problems of FDPSO were discussed.

By selecting the 2000 m water depth environmental condition as the research background, Sun et al. (2015) designed a set of equal angle averaged-distributed taut mooring system for an octagonal FDPSO, and carried out the numerical calculation basing on the linear frequency domain analysis. This study found that compared with the catenary mooring system, the taut mooring system has a lighter weight, which enhances the oil storage capacity of FDPSO. Moreover, the taut mooring system has smaller radius, which can save seabed resources and facilitate the operation of oil pipeline laying. In addition, after the broken of one chain, the taut mooring system possesses more effective ability of mooring positioning than catenary mooring system.

Considering the influence factors such as the draft depth, the number, and the width of the heave plates, as well as the spacing between the heave plates, Yu et al. (2016) used SESAM software to carry out a detailed study on the performance of FDPSO with different parameters of heave plate. Ultimately, the optimal parameters were obtained. The results revealed that the natural periods of the heave and pitch motion of FDPSO can be greatly changed by the arrangement of the heave plates. Within a certain range, the natural period of the heave motion increases with the number of the plate, the width of the plate and the spacing between the plates. The width of the plate has the greatest influence on the natural period. However, the change of the draft depth of the single layer heave plate has a very small impact on the performance of the platform.

Yao et al. (2016) and Wang et al. (2016) proposed a new FDPSO with a sandglass-type floating body and advised a suitable analysis method based on the hydrodynamic performance of the floating model. The effects of different mooring parameters and shape parameters on the motion performance of FDPSO are studied by using classic boundary element method based on potential theory. Some principles for designing the mooring scheme of the new type of FDPSO in deep water which satisfied the DNV classification society requirements are also proposed. By combining numerical simulation and model test, Gu et al. (2012; 2013; 2015) analyzed the dynamic response and calculated the tendon tension of the mooring system of a tension leg platform (TLP). The six-degree-of-freedom dynamic coupling responses and the mooring characteristics of TLP under random waves are studied by using a self-developed program.

Wang et al. (2013) proposed a new model and an optimization method for the underwater rotating technology used in floating non-traditional manufacture of cylindrical shape FDPSO. The Sevan Driller FDPSO manufactured by COSCO (Nantong) Shipyard Co., Ltd in China was employed as example in his study. Liu et al. (2011) discussed the design idea, production mode and equipment configuration of two FDPSOs named Azurite and MPF1000. Azurite is the world's first FDPSO and MPF1000 is still being built now. In addition, many scholars such as Wei et al. (2011) and Li et al. (2013) put forward some new conceptual designs for FDPSO and carried out the research work on the hydrodynamic performance and mooring characteristics.

In this paper, the coupling effects between hull and mooring system, floating box and columns are taken into account. Considering the operation and self-survival conditions, as well as the 0° and 45° wave direction, there are four kinds of working conditions. Complementarily, an equivalent truncated mooring design method is adopted. Particularly, the 6-DOF motions series, the tension statistical characteristics, spectrum rules, cable strength check of the 16 mooring lines are carried out in detail. The purpose of this paper is to provide some reference for the study of hydrodynamic performance and mooring system characteristics on the new deep draft multi-column FDPSO.

II. DESCRIPTION OF THE FDPSO AND MOORING SYSTEM

1. Features of the New Type of Deep Draft Multi-Column FDPSO

The general arrangement of the new type of FDPSO is shown in Fig. 2. The dimensions and hydrodynamic parameters are listed in Table 1. The hull of the FDPSO consists of an octagonal buoyancy structure (pontoon) and four columns. There are four horizontal braces connecting the columns. Water ballast tanks, oil storage, solid ballast and four lower pump rooms are arranged in the pontoons. Upper pump rooms, voids, water ballast, oil storage, diesel oil, mud, potable water, drilling water and base oil tanks are arranged in the columns. In addition, there are four horizontal access tunnels inside the pontoons connecting the pontoon lower pump rooms. The seawater is displaced through a buffer cell in the pontoon. There is one buffer cell for two oil storage tanks located in the pontoon. The displaced seawater is sampled before discharged to sea. The water contaminated by oil will be transferred to topside for water treatment.

2. The Arrangement of the Mooring System and Equivalent Truncation Design

The FDPSO's mooring system is composed of 4 groups and a total of 16 chain-polyester-chain type mooring lines. In each group, the interval angle between adjacent mooring lines is 5°, as shown in Fig. 3. Distance between anchor and the center of platform is 2440 meters. The parameters of mooring system are displayed in Table 2.

For the prototype, the operating depth is 1500 m, and the distance between fairlead and waterline plane is 51.5 m. Even

Table 1. Main dimensions and hydrodynamic parameters of FDPSO.

Designation	Unit	Parameters	Designation	Unit	Parameters
Length	m	81.8	width of pontoon under the column	m	20.02
Width	m	81.8	width of pontoon between columns	m	19.056
Depth	m	76.5	Pontoon height	m	10.92
Maximum water depth	m	1500	Longitudinal center of gravity position	m	0/0
Draft of operation/self-survival	m	59.15/59.15	Vertical center of gravity position	m	25.52
Displacement	t	119,660	Inertia radius of pitching	m	31.84
Total height of column	m	64.08	Inertia radius of roll	m	30.56
Bottom diameter of column	m	20.02	Inertia radius of yaw	m	32.4

Table 2. Configuration of the mooring lines in prototype.

Designation	Length	Diameter	Weight in air	Submerged Weight	Axial stiffness	Minimum breaking load
Unit	m	mm	kg/m	kg/m	kN/m	kN
Chain	2514	127	321.86	279.82	1,623,600	14, 955
Polyester	319	262	42.44	10.57	468, 396	17, 348

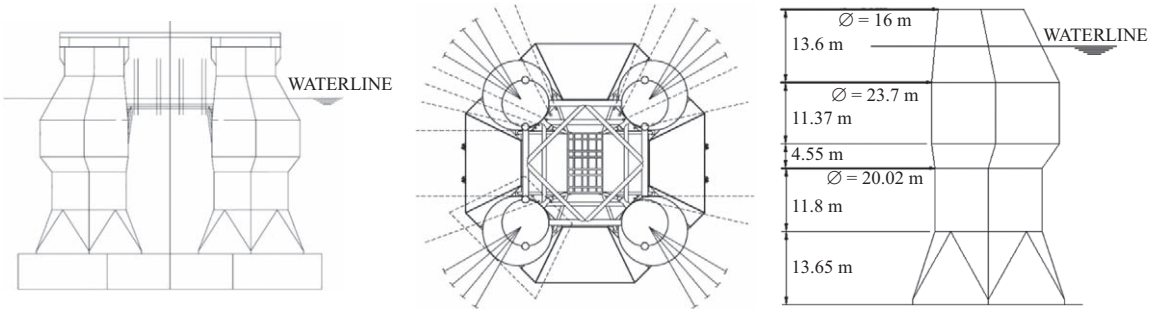

Fig. 2. General arrangement of the FDPSO.

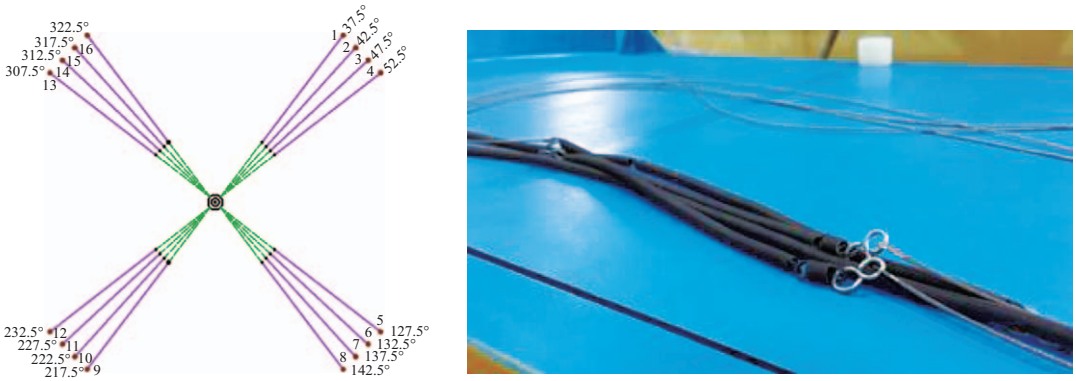

Fig. 3. Arrangement of the mooring lines and the model of the truncated mooring lines.

though the scaling factor is 1:80, the model's mooring system is too large for the basin. Therefore, it is necessary to adopt equivalent truncation mooring system. In the equivalent truncation design, Stansberg et al. (2002) has gave the detailed introduction for the method of truncated system's selection and design. According to his research production, the following principles must be obeyed: Model the correct total, horizontal restoring force characteristic; Model the correct quasi-static coupling between vessel responses; Model a representative level of mooring and riser system damping, and current force; Model representative single line tension characteristics (at least quasi-static). The vertical truncation factor of mooring ropes is 5 ($\gamma = 5$). The mooring lines of model are made up of mini-chain and spring. More details of the mooring lines system after being

Table 3. Parameters of the mooring line in truncated model.

Designation	Length		Submerged Weight		Axial stiffness		Pre-Tension	
	Prototype	Model	Prototype	Model	Prototype	Model	Prototype	Model
	(m)	(m)	(kg/m)	(kg/m)	(kg × 10^6)	(cm/kg)	(kN)	(kN)
Chain	60	0.750	2740	0.0426	165.31	0.238		
Polyester	262.395	3.280	1324.446	0.0206	4.11	41.895	3754.27	0.7295
Chain	80	1.000	2740	0.0426	165.31	0.318		

Table 4. Environment parameters of wind, wave and current.

Load case	Significant wave height (m)	Peak period (s)	Current Speed (m/s)	Average wind speed (m/s)
self-survival condition	12.19	14.6	1. 5	24.2
operation condition	3.96	9.0	0.85	38.6

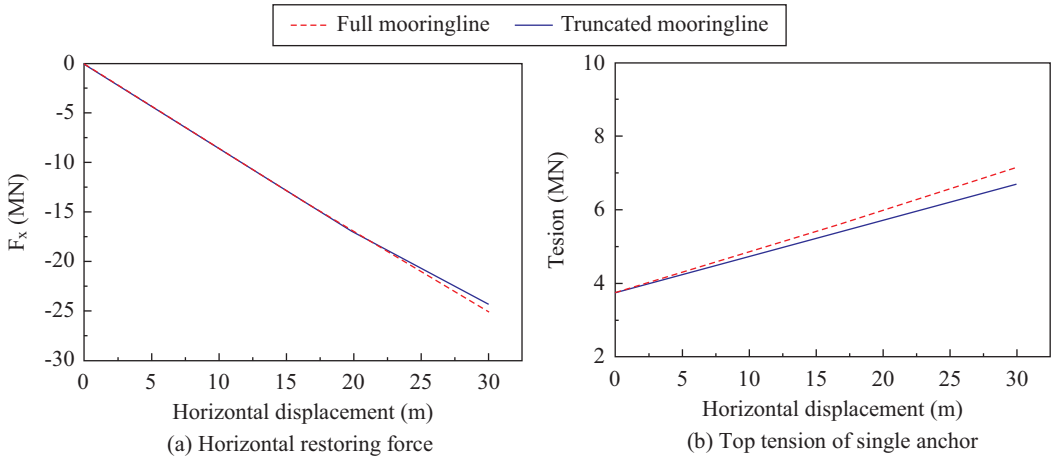

Fig. 4. Force characteristics of mooring system before and after truncation.

truncated are presented in the Table 3.

The spring is used to simulate the actual mooring line's axial stiffness. In order to get the same wave and current forces as the full water depth experiment, there is sufficient length of mini-chains in the upper end of the mooring ropes.

The static force characteristics of the complete mooring system (full or truncated) are displayed comparatively in Fig. 4(a). The tension characteristics of single mooring line (full or truncated) are shown in Fig. 4(b). From Fig. 4, we can find: before and after equivalently truncated, the horizontal restoring force characteristic of whole mooring system and the top tension characteristic of single mooring line are roughly the same.

3. Ocean Environment and Working Conditions

The random wave component is described by the Jonswap spectrum, and overall cyclic current is adopted to simulate actual current loads. The prototypical FDPSO is used to operate in Gulf of Mexico. The wind, wave and current parameters of 1-year return period and 100-year return period in operating sea area are respectively applied as its operation condition and self-surviving condition. The wind, wave and current parameters are shown in Table 4. The profile type of current is determined to be steady flow in the model test. The wind load is simulated through acting on constant external force at centroid of windward surface of FDPSO. The target wave spectrum and the actually generated experimental wave spectrum are shown in Fig. 5.

III. NUMERICAL MODELING

In this study, numerical simulations are carried out in time domain. Compared with the wavelength, the columns and the pontoons are large-scale structures. Hence, the potential flow theory is adopted to calculate the wave hydrodynamic information involving first order hydrodynamics. The fluid needs to satisfy the Laplace's equation:

$$\nabla^2\phi^{(1)} = \frac{\partial^2\phi}{\partial x^2} + \frac{\partial^2\phi}{\partial y^2} + \frac{\partial^2\phi}{\partial z^2} = 0 \tag{1}$$

where $\phi^{(1)}$ is first order total velocity potential function including the incident potential $\phi_I^{(1)}$, diffraction potential $\phi_D^{(1)}$,

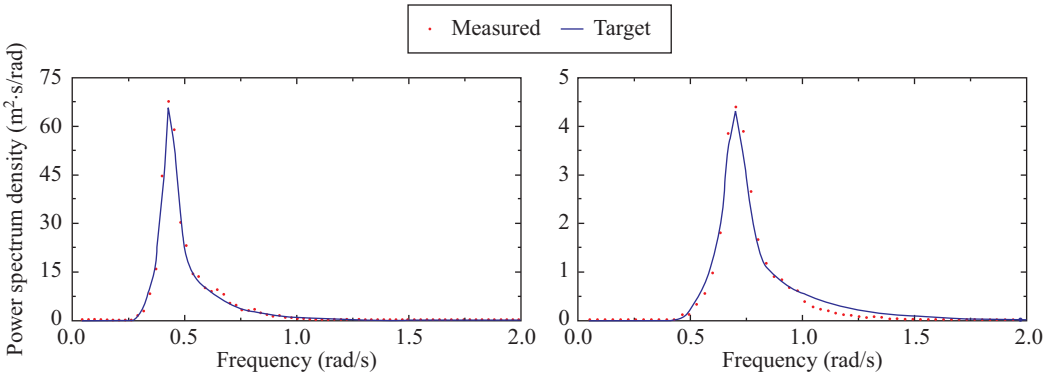

Fig. 5. The target wave spectrum and the actual experimental wave spectrum.

and radiation potential $\phi_R^{(1)}$. By solving the resulting boundary-value problem, the potential function $\phi^{(1)}$ is solved. The six components of the force and moment vectors are obtained through the direct integration over the wetted body surface (S_H):

$$F_k = \mathrm{Re}[-\rho a e^{-i\omega t}\iint_{S_H} n_k(\phi_I^{(1)} + \phi_D^{(1)})ds] \quad (k = 1, 2, 3) \quad (2)$$

$$F_k = \mathrm{Re}[-\rho a e^{-i\omega t}\iint_{S_H} (r \times n)_k(\phi_I^{(1)} + \phi_D^{(1)})ds] \quad (k = 4, 5, 6) \quad (3)$$

where ρ is the water density, a is the incident wave amplitude. k = 1, 2, 3, …, 6 denote the models, specifically the surge, sway, heave, roll, pitch, and yaw. S_H is the wetted body surface. The frequency-dependent added mass and damping coefficient matrixes of the floating body with the restriction can be expressed as:

$$F_R^{(1)} = \mathrm{Re}\, M^a\{\ddot{\xi}^{(1)}\} + C\{\dot{\xi}^{(1)}\} \quad (4)$$

where M^a and C are added mass and damping matrixes. $F_R^{(1)}$ is the radiation force vector and calculated by using radiation potential $\phi_R^{(1)}$. And the motion equations of time domain analysis for the FDPSO are described as follows:

$$\begin{aligned}&[M + a(\infty)]\{\ddot{\xi}\} + \int_{-\infty}^{t}[h(t-\tau)]\{\dot{\xi}\}\,\mathrm{d}t + K\{\xi\} \\ &= F^{wave} + F^{current} + F^{wind}\end{aligned} \quad (5)$$

where M is the generalized mass matrix for the FDPSO, $a(\infty)$ is the infinite frequency-added mass, K is the hydrostatic restoring stiffness matrix. F^{wave}, $F^{current}$ and F^{wind} denote the wave drag force, the current drag force, and the wind drag force, respectively. $h(t)$ is retardation function matrix, which means the influence of the memory effect in the free surface. It can be obtained by the following equation:

$$h(t) = \frac{2}{\pi}\int_0^{\infty}\lambda(\omega)\cos\omega t\,\mathrm{d}\omega \quad (6)$$

It should be noted that the damping on the FDPSO from viscous skin drag, wave drift damping and radiation damping should be also included in the item of $\int_{-\infty}^{t}[h(t-\tau)]\{\dot{\xi}\}\,\mathrm{d}t$ by the form of critical damping, because these variants are related to the motion velocity of the FDPSO.

1. Irregular Wave Modeling

In order to reproduce model test wave conditions as accurately as possible, a time history series of wave elevation was measured by the monitoring points set in the basin. Then, the time series will also generate a user-defined spectrum by using a Fast Fourier Transform (FFT), whose frequency range is based on a JONSWAP fit of the wave elevation spectral density. Within the frequency range of the fitted spectrum and subject to the limitations of roundoff error, the wave elevation time-history in our numerical calculation will be expressed as exactly by multiplying each of the spectral wavelets. The model assumes that the sea comprises finite regular waves at a random phase.

$$\eta(t, x) = \sum_{i=1}^{N} A_i\cos(k_i x - \omega_i t + \varepsilon_i) \quad (7)$$

where N is the number of spectral lines, i is the wavelet number, t is time, ω is frequency, ε is phase, A_i is the wavelet amplitude, k is the wave number.

Beside the first order issues, slow drift motion of low frequency has been proven which is also important for a moored floating platform. 2nd order wave slow drift force in the procedure is predicted by using Newman's approximation.

$$F_{sv}(t) = 2[\sum_{i=1}^{N} A_i(T_{ii}^{ic})^{\frac{1}{2}}\cos(\omega_i t + \varepsilon_i)]^2 \quad (8)$$

Table 5. Variables between the prototype and model.

Item	Symbol	Scale Ratio
Linear dimension	L_s / L_m	λ
Linear velocity	V_s / V_m	$\lambda^{1/2}$
Angle	$\varnothing_s / \varnothing_m$	1
Period	T_s / T_m	$\lambda^{1/2}$
Area	A_s / A_m	λ^2
Volume	∇_s / ∇_m	λ^3
Moment inertia	I_s / I_m	$\gamma\lambda^5$
Force	F_s / F_m	$\gamma\lambda^3$

where T_{ii}^{ic} and ε_i are 2nd wave force transfer functions of different frequencies and phases.

2. Wind and Current Loads

In this paper, the current force coefficients are used to calculate the viscous drag force of the current on the hull of this FDPSO, which are defined as the force or moment per unit velocity squared. For each direction of the current (-180 to +180 degrees), there are the X force coefficient (Translation X), Y force coefficient (Translation Y), Z force coefficient (Translation Z), Rotation about X coefficient (Rotation X), Rotation about Y coefficient (Rotation Y), and Rotation about Z coefficient (Rotation Z). For relative current velocity U in direction ϕ:

$$\begin{aligned} &\text{Force in X direction} = CFX_\phi \cdot U^2 \\ &\text{Force in Y direction} = CFY_\phi \cdot U^2 \\ &\text{Moment about Z axis} = CRZ_\phi \cdot U^2 \end{aligned} \tag{9}$$

where *CFX*, *CFY* and *CRZ* are the coefficients. Similar equations apply for force in Z and moments about X and Y. Note that the forces are in the directions of the axes, not in the direction of the current. The wind force is similar to wind, a type of drag force.

IV. EXPERIMENTAL SETUPS

This experiment was carried out in the State Key Laboratory in Shanghai Jiaotong University. Testing time for each case in the model test was defined corresponding to 3 hours in prototype. The scaling factor of the model is 1:80. The dimensions of the basin are 50 m × 30 m × 6 m. According to the scaling factor 1:80, the water depth is set at 3.75 m corresponding to the prototyped truncated water depth of 300 m. In the present tests, the Froude number and Strouhal number of the model and prototype were kept in the same, which means the similarity of the gravitational force and inertia force is satisfied. Based on the law of similarity, the relationships of physical variables between the prototype and model are listed in Table 5, where λ means linear scale ratio and γ means specific gravity of seawater (γ = 1.025).

Fig. 6. Nozzle of the current generating system.

The main body of the model is made of plexiglass. The FDPSO model is hollow for adjusting gravity center easily. The FDPSO model is painted with waterproof material for protecting structural strength and water resistance. To capture the same hydrodynamic performance with the actual FDPSO, it is crucial to set correct displacement, exact gravity center position and inertial radius. The gravity center position is adjusted through changing the weights on inertial moment frame.

The current generating system is shown in Fig. 6. Internal circulation mode is adopted in the current generation system. High power pump draws the water in the pool through the pipeline. The high-pressure water flow is ejected from the nozzle of the pipes through the pressure of the water pump. Because a plurality of nozzles are arranged evenly on each pipe along the width direction of the pool, the water jet out from pipes is relatively uniform, which forms a uniform and stable flow of water inside the basin.

The environment conditions were calibrated before having the model tests. The time series of the random wave elevations and the frequency spectrum of the dynamic response are generated through the algorithm of FFT, while these are not necessary for the wind and current. The 6-DOF motion responses of the new type of deep draft multi-column FDPSO, the time traces of the mooring lines loads and the acceleration at the center of the deck are measured during the model test. The data were captured with a sampling frequency of 4.75 Hz. A photo of the FDPSO in the operation condition under the combined action of the wave, wind and current is shown in Fig. 7. All of the measured data in the model tests have been extended to the full scale in this study.

V. MOTION RESPONSES AND MOORING CHARACTERISTICS OF FDPSO IN WIND, WAVE AND CURRENT

1. Natural Period and Dimensionless Damping Coefficient of the FDPSO

A free decay experiment is carried out to determine the platform's natural period and damping parameters. In this experiment, no environmental load but initial displacement or initial rotation angle are exerted on the platform. Through analyzing the damping curve of each freedom motion, the natural period and damping coefficient of platform's motion are gained. The results are exhibited in Table 6. The FDPSO will have a cancellation of heave for some wave periods. This is caused by sum-

Table 6. Natural period and dimensionless damping coefficient of FDPSO and several typical offshore platforms.

Designation		Surge	Sway	Heave	Roll	Pitch	Yaw
New type of FDPSO	Natural period (s)	99.11	99.11	24.29	34.96	34.96	**55.36**
	Dimensionless damping coefficient	0.0352	0.0352	0.0144	0.0219	0.0219	0.0183

Table 7. Summary of motion statistics of the FDPSO in operation and self-survival condition.

Designation		Operation condition				Self-survival condition			
		Max	Min	Mean	STD	Max	Min	Mean	STD
Surge (m)	0°	1.053	-7.123	-2.394	1.001	2.262	-12.45	-5.230	2.380
	45°	-1.349	-4.425	-2.697	0.475	2.255	-8.814	-4.085	1.466
Sway (m)	0°	2.467	-1.740	0.133	0.655	2.668	-3.000	0.137	0.649
	45°	4.107	1.038	2.573	0.527	9.486	-1.292	4.215	1.527
Heave (m)	0°	-0.003	-0.462	-0.212	0.058	1.563	-3.143	-0.313	0.621
	45°	0.204	-0.375	-0.037	0.108	1.726	-2.855	-0.204	0.623
Pitch (deg)	0°	1.634	-2.321	-0.370	0.488	2.729	-5.786	-1.695	1.075
	45°	0.034	-1.087	-0.547	0.161	0.046	-3.583	-1.691	0.402
Roll (deg)	0°	0.426	-0.376	0.020	0.107	0.724	-0.479	0.076	0.154
	45°	0.196	-1.497	-0.635	0.158	0.005	-3.673	-1.788	0.447
Yaw (deg)	0°	0.902	-0.768	0.014	0.242	1.357	-1.104	-0.052	0.352
	45°	0.397	-0.814	-0.118	0.177	0.776	-0.958	-0.107	0.274

Fig. 7. Model test of FDPSO in the State Key Laboratory of Ocean Engineering.

mations of the mass force and pressure force components, which are similar in size but present opposite phase to these periods. The mass contribution comes mainly from the pontoons while the pressure contribution comes from the columns.

2. Characteristics of Motion Responses

The time series of 6-DOF motion responses are shown in Fig. 8. The statistical datas of platform's motion responses such as the maximum, minimum, average value and standard deviation are shown in Table 7.

As shown in Fig. 8, the motion responses in self-survival condition are more severe. In self-survival condition, the mean value of the surge reaches 5.23 m, and the maximum value is 12.45 m. Under 0° wave direction, the platform mainly oscillates around the initial position, and the mean values of sway in two kinds of working conditions are basically identical. The statistical data of heave motion response under different wave directions is relatively close, indicating that the wave direction has little effect on the heave motion of this new multi-column FDPSO. However, in the self-survival condition, the amplitude of the heave reached 3.143 m, which is far greater than the operating condition one. Under the 45° wave direction, the roll and pitch motions of FDPSO are influenced by the symmetry feature of platform structure, so the motion rules of them are basically similar, which is a particularly evident in the self-survival conditions. The maximum rolling angle appears under the 45° wave

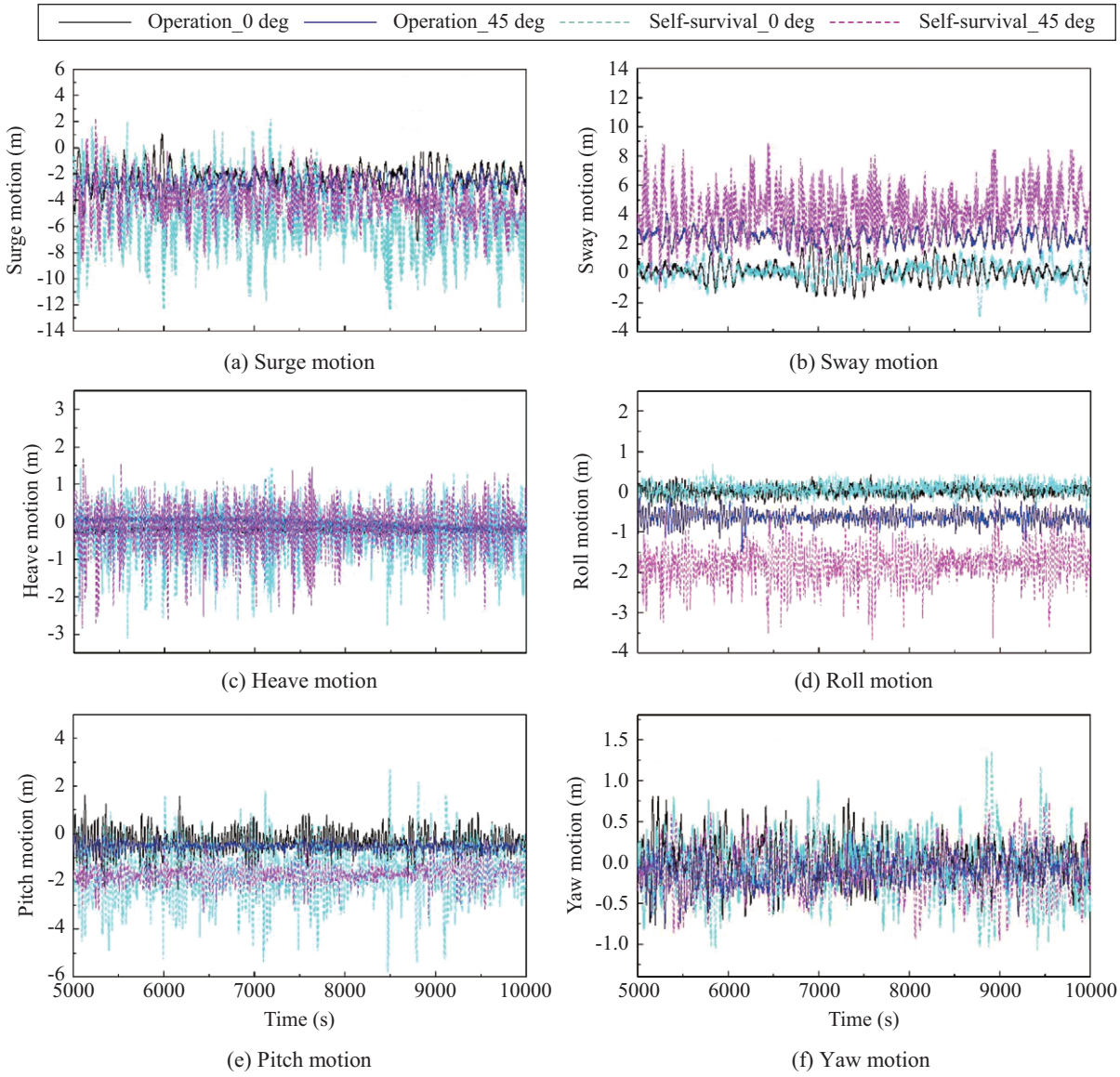

Fig. 8. Time series of the motion responses for the FDPSO in operation and self-survival condition.

direction in the self-survival condition, which is 3.673°. Due to the symmetry feature of the platform structure, the yaw motion has low sensitive to sea conditions and wave directions. In the operating condition, the maximum yaw angle is 0.902°. Even in the self-survival condition, the maximum yaw angle is only 1.357°, which shows that this new type of deep draft Multi-column FDPSO has good yaw motion performance.

The ocean structure's motion responses are a steady random process. Through statistical method, intuitive motion performance can be concluded, but the frequency-domain characteristics can not be discovered. In order to analyze the distribution of different frequency components, spectrum analysis method is adopted.

The frequency spectra of 6-DOF motions responses in self-survival condition are shown in Fig. 9. The spectra statistical data of 6-DOF motions responses in operation and self-survival condition are presented in Table 8. The peak frequency of wave spectrum is 0.43 rad/s, the natural frequency of surge is 0.063 rad/s, and the natural frequency of the heave is 0.259 rad/s. From Fig. 9, we can discover that frequency spectra of surge motion and heave motion display double-peak feature. The frequencies corresponding to the two spectrum peaks of the surge motion are 0.065 rad/s and 0.432 rad/s, respectively. The frequencies corresponding to the two spectrum peaks of the heave motion are 0.262 rad/s and 0.432 rad/s, respectively. It can be inferred that for surge and heave motion, one peak frequency is located at the peak frequency of wave spectrum, and another peak appears near the natural frequency. For the surge motion, the spectral density near the natural frequency is larger than that near the peak frequency of wave spectrum. However, the spectral density of the heave motion is opposite to the surge motion, which proves that the heave motion is more susceptible to the

Table 8. Spectrum characteristics of the FDPSO in operation and self-survival condition.

	Designation		Surge	Sway	Heave	Roll	Pitch	Yaw
Self-survival condition	0°	Peak frequency (rad/s)	0.065/0.432	0.065	0.262/0.432	0.175	0.171	0.114
		PSD*	99.622/22.555	13.643	2.087/3.558	0.273	29.445	2.418
	45°	Peak frequency (rad/s)	0.063/0.413	0.064/0.415	0.256/0.412	0.178	0.182	0.117
		PSD	40.841/12.618	37.42/15.577	1.324/4.681	4.181	3.018	2.843
Operation condition	0°	Peak frequency (rad/s)	0.074	0.06	0.264	0.060/0.176	0.075/0.186	0.075/0.118
		PSD	35.785	37.7	0.068	0.175/0.166	1.495/5.575	0.600/1.620
	45°	Peak frequency (rad/s)	0.067	0.063	0.265	0.073/0.191	0.074/0.192	0.052/0.117
		PSD	8.047	12.258	0.052	0.105/0.713	0.175/0.672	0.156/0.497

* The unit for the surge, sway and heave motion is $m^2 \cdot s/rad$; the unit for the roll, pitch and yaw motion is $deg^2 \cdot s/rad$).

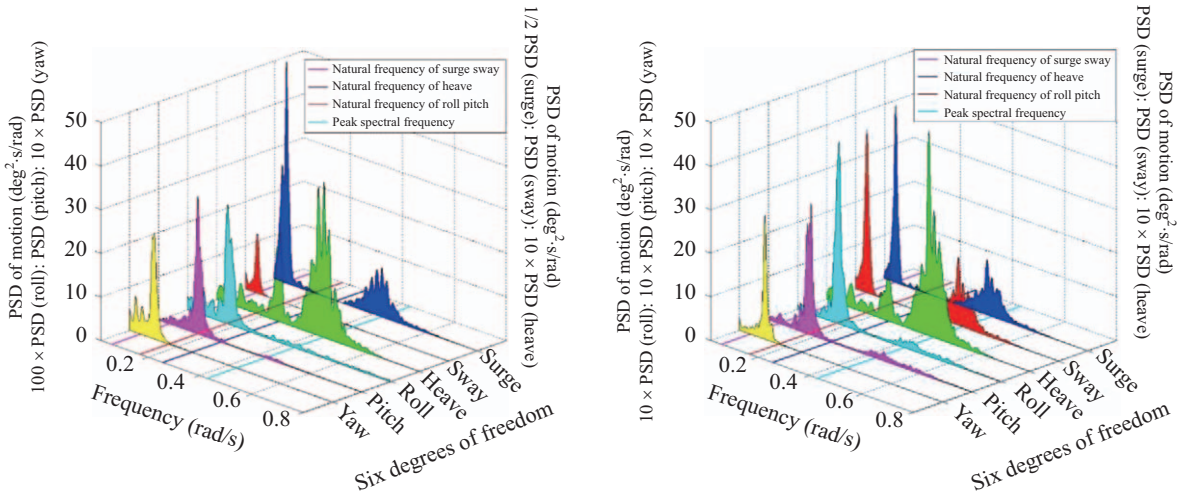

(a) wave direction of 0^0 (b) wave direction of 45^0

Fig. 9. Spectrum characteristics of 6-DOF motion responses in self-survival condition.

waves. For sway, roll, pitch and yaw, there is only one peak. The frequencies corresponding to the spectra peaks of the sway, roll, pitch and yaw motions are basically close to the natural frequency. The natural frequency of the sway, roll, pitch and yaw motions are 0.063 rad/s, 0.180 rad/s, 0.180 rad/s and 0.114 rad/s, respectively.

Additionally, the frequency spectrum curves of surge, heave, roll, pitch, and yaw under 45° wave direction show the similar law to that of 0° wave direction. The sway motion under 45° wave direction also displays the double-peak feature. The frequencies corresponding to the two peaks are 0.064 rad/s and 0.415 rad/s, which are close to the natural frequency of the sway motion and the peak frequency of the wave spectrum, respectively. Due to the symmetry of the platform structure, under 45° wave direction, the tendency of frequency spectrum curve of sway is basically the same as that of surge.

There is a difference between the self-survival condition and operation condition in the spectra characteristics of FDPSO 6-DOF motions. The spectrum response characteristics of 6-DOF motions in operation condition are shown in Fig. 10. Overall, in operation condition, the surge, sway and heave display single peak, while roll, pitch and yaw display double-peak feature. The peak frequencies of the surge, sway and heave is close to the natural frequency of themselves, which means that the effect of wave force on the platform is small at this time. For roll, pitch and yaw motion spectra, one peak frequency appears near the natural frequency, while another peak frequency presents in the low-frequency region and gets close to the natural frequency of the surge and sway, which is possibly caused by the coupling effects of roll and sway, pitch and surge.

3. The Tension of FDPSO's Mooring System

According to the specification API-RP-2SK (2005), for full mooring system, when using quasi-static analysis design, the safety factor of maximal mooring line tension is 2.0. When using dynamic analysis design, the safety factor of mooring-line tension is 1.67. In this experiment, dynamic analysis design is applied for the full mooring system. The safety factor of each mooring-line should be no less than 1.67.

Each mooring line of this model is composed of the polyester cable and the steel-chains at both ends. The polyester's design strength is better than steel-chain. Moreover, the mooring-

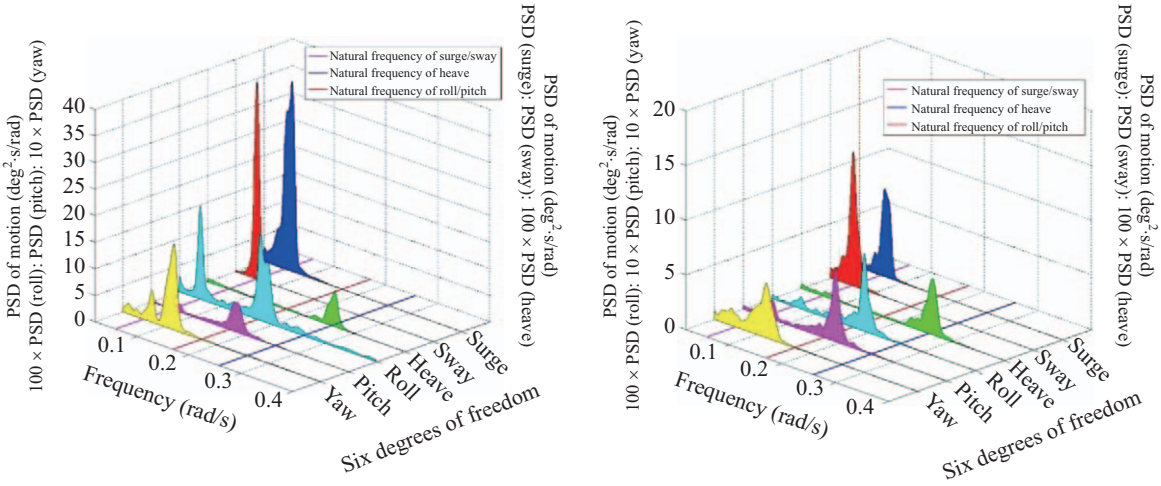

(a) wave direction of 0° (b) wave direction of 45°

Fig. 10. Spectrum response characteristics of 6-DOF in operation condition.

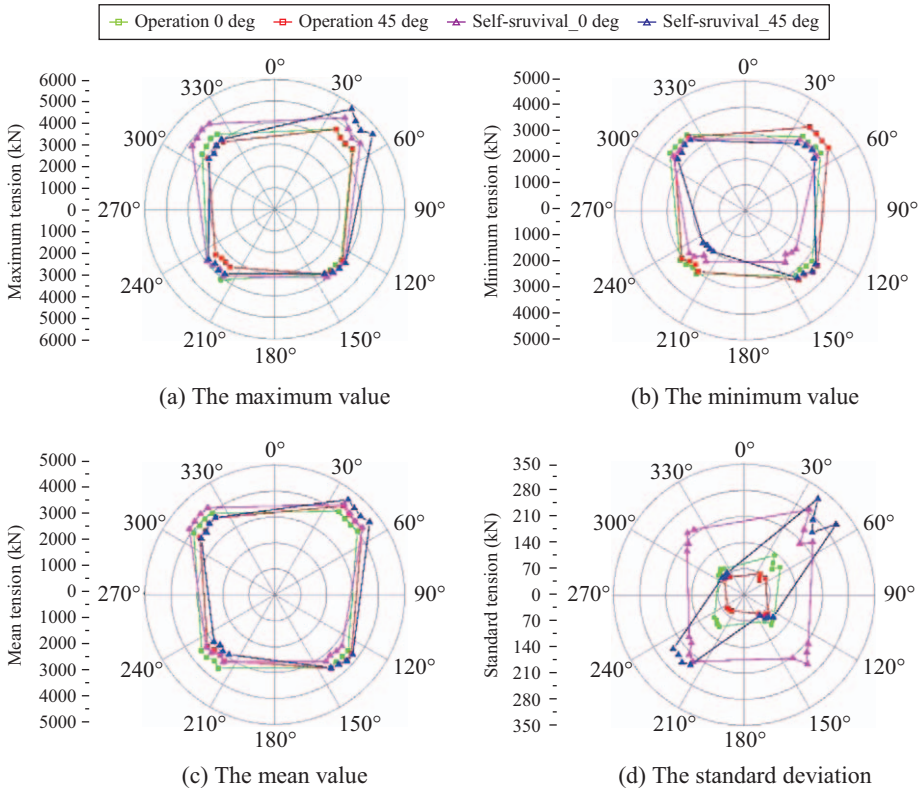

(a) The maximum value (b) The minimum value

(c) The mean value (d) The standard deviation

Fig. 11. Tension characteristics of mooring system for operation and self-survival condition.

line tension decreases with the increase of water depth. Therefore, the security factor of the steel-chain near fairlead should be determined to check the mooring system's reliability.

Fig. 11 shows the statistical characteristic of mooring lines in self-survival and operation conditions. Overall, the maximum value, the minimum value and the average value of the four mooring lines of each group are basically the same. In both two kinds of wave direction, the tension of upstream mooring line is greater than that of downstream mooring line significantly. Whether in the self-survival condition or operation condition, the maximum tensions of chain No.5-No.8 are less affected by wave directions, and the maximum tensions of chain No. 13-No. 16 under the 0° wave direction are greater than those under 45° wave direction. From Fig. 11(a), we can see that the maximum tension occurs at the No. 1 mooring line under 45° wave direction in self-survival condition. In self-survival condition,

Table 9. Safety factor of mooring line.

Load case	Wave direction (deg)	Mooring line No.	Maximum tension value (kN)	Safety factor
self-survival condition	0	#1	5320.25	2.811
	45	#1	5844.05	2.559
operation condition	0	#1	4666.07	3.205
	45	#1	4648.16	3.217

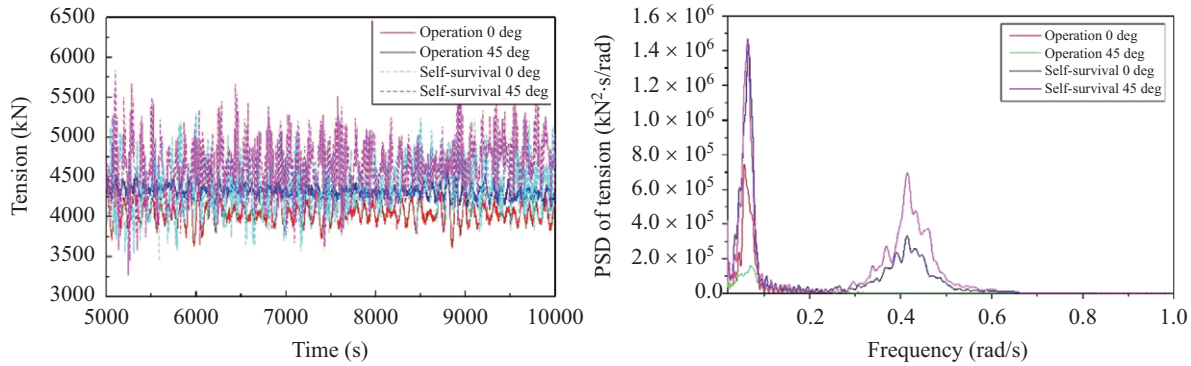

Fig. 12. Time series of tension and power density spectrum for No.1 mooring line.

the maximum tension of upstream mooring line increases more significantly, which indicates greater failure risk.

Fig. 11(c) and Fig. 11(d) display the mean value and standard deviation of tensions. The mean tensions of upstream mooring lines in self-survival condition are greater than that of operation condition, while mean tension of downstream mooring lines in self-survival condition is smaller than that of operation condition. This phenomenon is caused by that the equilibrium positions in self-survival is closer to the downstream. Under 0° wave direction of self-survival condition, the tension standard deviations of four mooring lines for each group shows great difference. Under 45° wave direction of self-survival condition, the tension standard deviations of four upstream mooring lines and four downstream mooring lines are much greater than the eight beside ones. Therefore, in self-survival condition, tensions of mooring lines along flow direction fluctuate severely.

The tension distribution under 45° wave direction is more concentrated compared with that under 0° wave direction, indicating greater failure risk. Table 9 displays the security factor of mooring-line's maximum tension. The safety factors of mooring lines are higher than the allowable values, showing sufficient strength margin in the mooring system.

Fig. 12 shows the time series of tension and power density spectra for No. 1 mooring line in four typical conditions. As shown, under 45° wave direction, the tension change of mooring system in self-survival condition is the most violent. In operation condition, the tension has the smallest pulsation around the average value. The power density spectrum of the top tension in each condition is shown in Fig. 12, too. The tension spectrum curve shows two peaks in self-survival condition, one is located at low-frequency, and the other is located at the peak frequency of the wave spectrum. However, in operating conditions, there is only a low-frequency peak. In self-survival condition, the power spectrum density (PSD) at low-frequency is larger than the wave frequency one, similar to the above mentioned performance of surge motion. In operation condition, the low-frequency peak is obvious, but the wave frequency peak almost disappears, the PSD curve's changing trend is almost identical to the performance of surge motion. It is believed that the low-frequency motion mainly contributes to the increase of tension. Then, we conduct an in-depth discussion for this phenomenon in the following sections.

VI. NUMERICAL SIMULATION RESULTS

In order to study the response mechanism of this FDPSO, the numerical simulation is carried out. By comparing the numerical simulation results with the experimental results, the accuracy of the numerical simulation results is verified firstly. On the base of these, this paper studies the effect of current velocity on the motion response of the platform in the self-survival condition.

1. Validation and Comparative Analysis

Due to the limitations of paper length, the numerical simulation results are chosen to compare with the experimental results only under 0° wave direction of the self-survival condition. Comparisons of the time series between the measured data and the numerical simulations were presented in this section, as well as the spectrum analysis.

In the presented analysis, the wind, wave, and current are assumed to move forward along the X-axis of the platforms. The geometry of this FDPSO is symmetrical in the X-axis and Y-axis.

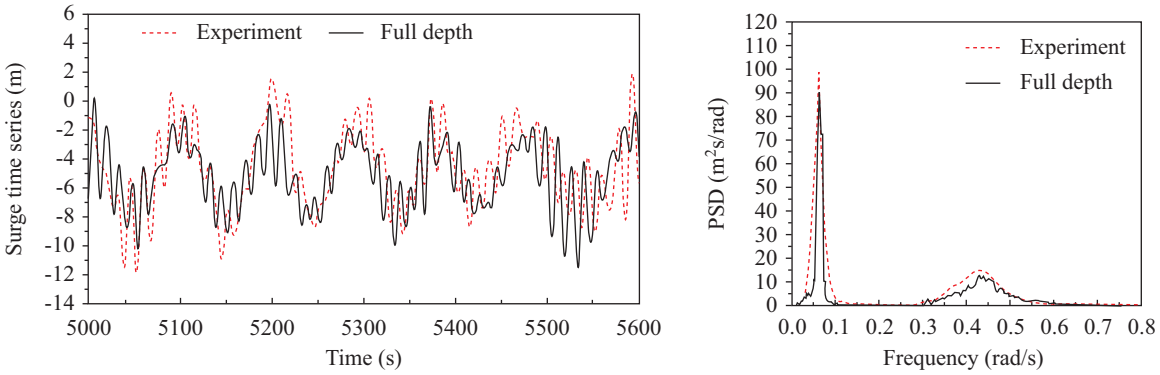

Fig. 13. Time series and power density spectrum for the surge motion.

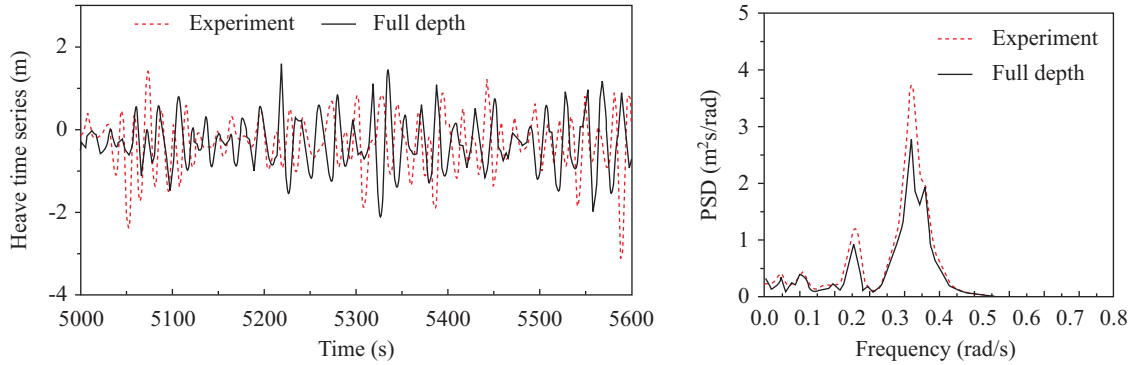

Fig. 14. Time series and power density spectrum for the heave motion.

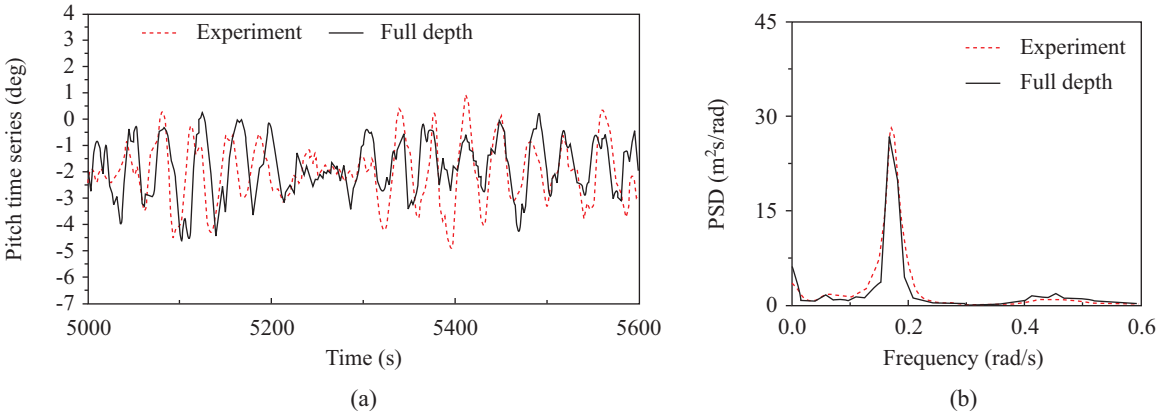

Fig. 15. Time series and power density spectrum for the pitch motion.

Therefore, only the surge, heave, and pitch response are discussed in this paper. Additionally, all the calculated results are regarded as the center of gravity. The numerical simulations with full depth mooring system and the experimental results with truncated mooring system are presented in Figs. 13-15. All the parameters in time series are partially presented from 5000 s to 5600 s in this paper for the light of more clear presentation.

The comparisons between numerical simulations and the experimental results show clearly that the numerical model estimates the surge, heave and pitch motions effectively. It seems that the motion amplitudes of the numerical simulations are less than the experiment results, while commendable agreement is obtained for the motion tendency. A possible explanation for

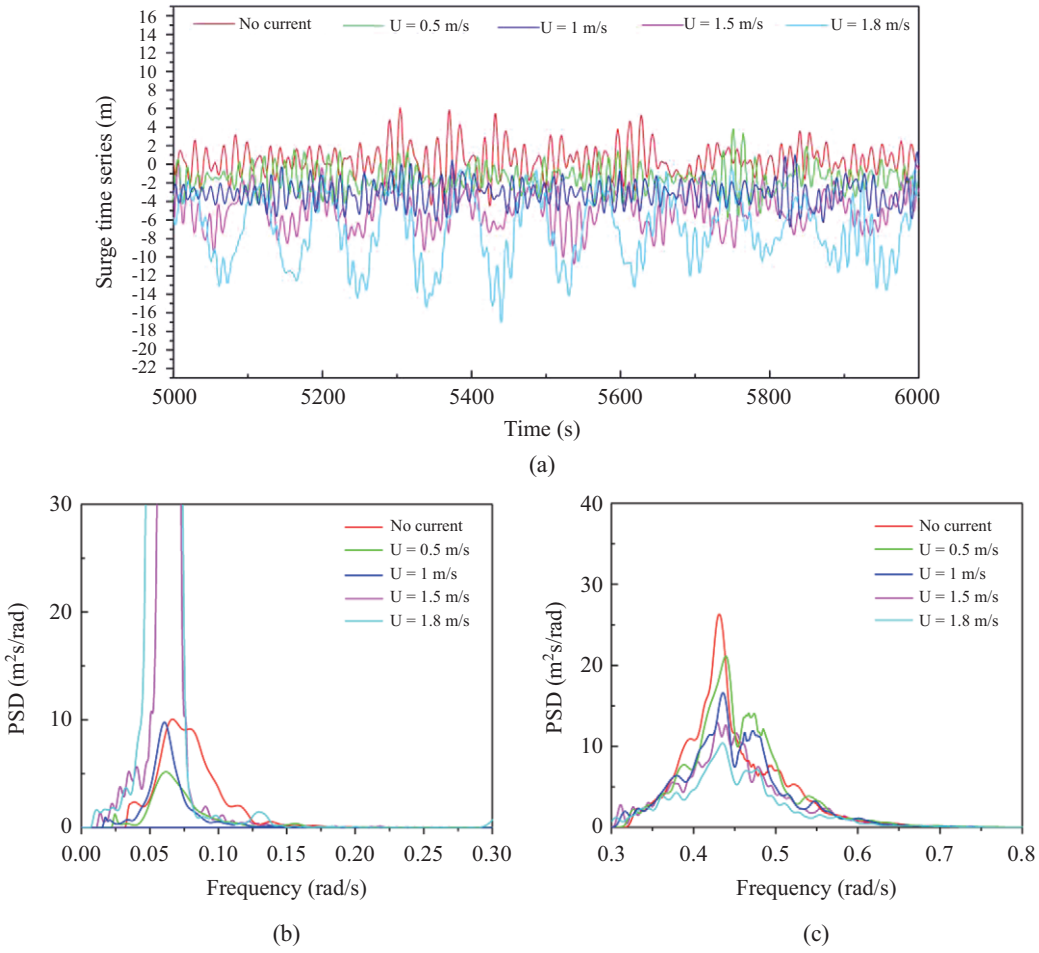

Fig. 16. Time series and power density spectra of the surge motion under different current velocities.

this phenomenon may be due to the reason that the slow-drift excitation in the numerical model is too small. The good agreement can also be seen in the response spectrum. Based on these, numerical simulation method is used to conduct further study.

2. The Effect of Current Velocity

Due to the variable cross section column, the drag forces are different along the length of column. Hence, the numerical simulation method is used to study the effect of current velocity on the surge motion response of the platform in the self-survival condition. We maintain the wind and wave load of self-survival condition, while current surface velocity is changed. The corresponding current surface velocities are 0, 0.5, 1, 1.5 and 1.8 m/s, respectively. Generally, moored platform motion is considered as a combination of W-F (water frequency) and L-F (low frequency) motion. However, actually the two types of motion can not be separated because dynamic response of W-F, L-F and mean offset are fully coupled. According to the fourth section of this paper, the surge motion shows obviously double-peak feature in self-survive condition. Therefore, only the analysis of the surge motion is selected here. The time series and power density spectra of the surge motion under different current velocities are presented in Fig. 16.

The Fig. 16(a) shows the time series of surge motion, while the Figs. 16(b) and (c) exhibit the L-F motion and W-F motion of surge, respectively. It is noted that current force not only makes a mean offset but also apparently suppresses the wave frequency motion in time domain analysis. As shown in Figs. 16(b) and (c), the surge motion of platform shows double-peak feature. At low current velocity, the peak spectral density of W-F motion is larger than the L-F motion one, which means that W-F motion dominates the surge motion at this time. The interesting phenomenon is that with the current velocity increasing from 0 to 0.5 m/s, both W-F motion and L-F motion decrease. Through de-coupling the W-F motion and L-F motion factitiously, Li and Ou (2010) obtained that the current significantly reduces the L-F dynamic response, which is consistent with the simulation result of this paper. This indicates that the method of separation motion analysis is effective at low current velocity. However, with the current velocity continuing to increase, the peak spectral density of L-F motion increased dramatically but the peak spectral density of W-F motion continues to decrease. The peak spectral density of L-F motion under U = 1.8 m/s reaches 328.4 m^2s/rad, which is far greater than

that under U = 1.5 m/s. This may be caused by that the maximal tensions of mooring system significantly increased at this point. Hence, as shown in Fig. 16(a), the system's natural frequency dominates the platform motion. This phenomenon verifies the results of the fifth section. These also illustrate that the method of separation motion analysis is not suitable for high current velocity, and the coupling relationship between the L-F motion and W-F motion must be taken into account.

In summary, the increase of current velocity can decrease the W-F motion of the platform's surge motion but makes the L-F motion firstly decrease and then increase. For the research object of this paper, there are relatively small L-F motion and W-F motion when the current velocity is 1m/s. Consequently, there is a current velocity satisfying the optimal surge motion of platform. In the future, we will study the mechanism of the influence of platform structure and mooring system on the optimal current velocity.

VII. CONCLUSIONS

In this paper, the model tests for a new type of deep draft multi-column FDPSO were carried out in the State Key Laboratory of Shanghai Jiao Tong University to investigate its hydrodynamic performance. A series of model tests at a scale of 1:80 were carried out with the truncated mooring lines. The free decay experiment and the dynamic response experiment under combined acting of wind, wave and current were conducted. The motion response performance and mooring system's tension characteristics are determined. Following conclusions can be obtained:

(1) In operation condition, the roll, pitch and yaw motion spectra display double-peak feature. For roll and pitch, one peak frequency appears near the natural frequency of themselves, while another peak frequency is close to the natural frequency of the surge and sway motions.
(2) In self-survival condition, the surge and heave motion spectra show double-peak feature. One peak frequency is close to the natural frequency of themselves, another is due to near the peak frequency of wave spectrum.
(3) The maximal tension of mooring system appears under the 45° wave direction in the self-survival conditions. In operation condition, tensions of mooring system are mainly caused by L-F force. In self-survival condition, W-F and L-F force both show obvious contribution, but the increase of tension is mainly caused by L-F force.
(4) A numerical simulation is adapted to verify that the truncated mooring system appears to effectively reproduce the characteristics of the full depth one. At the same time, the accuracy of numerical simulation is confirmed.
(5) The numerical simulation method is used to study the effect of current velocity on the surge motion response of the platform in the self-survival condition. The increase of current velocity can decrease the W-F motion of the platform's surge motion but makes the L-F motion firstly decrease and then increase.

VIII. ACKNOWLEDGEMENTS

This research is financially supported by the National Natural Science Found Project (51309123), the Open Foundation of State Key Laboratory of Ocean Engineering (1407) and the collaborative innovation center funded projects in Jiangsu University (High Technology Ship category).

REFERENCES

API-RP-2SK (2005). Design and analysis of station keeping systems for floating structures (third edition), American Petroleum Institute, October.

Gu, J. Y., J. M. Yang and H. N. Lv (2013). Numerical simulations and model tests of the mooring characteristic of a tension leg platform under random waves. China Ocean Engineering 27(5), 563-578.

Gu, J. Y., J. M. Yang and H. N. Lv (2012). Studies of TLP dynamic response under wind, waves and current. China Ocean Engineering 26(3), 363-378.

Gu, J. Y., X. Y. Zhu and J. M. Yang (2015). Numerical Study on the 3-D Complex Characteristics of Flow Around the Hull Structure of TLP. China Ocean Engineering 29(4), 535-550.

Korbijn, F., I. Husem and E. Pettersen (2005). OCTABUOY SDM, a compact semi-submersible design for deepwater applications, 2005-20021. Proceedings of 24th International Conference on Offshore Mechanics and Arctic Engineering June 12-17, Halkidiki, Greece.

Li, B. B. and J. P. Ou (2010). An effective method to predict the motion of DDMS platform with steel catenary riser. Proceedings of the 12th International Offshore and Polar Engineering Conference Beijing, China, June 20-25.

Li, Y., Y. G. Tang, Z. J. Zhao and Z. R. Wu (2013). Concept design and analysis of the mooring system for the new type of multi-tubular FDPSO. Chinese Journal of Ship Research 8(5), 97-103. (in Chinese)

Liu, J., B. Xie, X. C. Yu and Z. M. Yin (2011). The elementary analysis of the application of FDPSO in the development of deepwater oil field. Proceedings of the fifteenth China Marine (Offshore) Engineering Symposium; China Shanghai, 132-136. (in Chinese)

Stansberg, C. T., H. Ormberg and O. Oritsland (2002). Challenges in Deep Water Experiments: Hybrid Approach. Journal of Offshore Mechanics & Arctic Engineering 124(2), 90-96.

Sun, Q., Q. H. Dong, G. S. Peng, T. Tian, B. Xie, S. S. Wang, X. C. Yu and J. R. Zhao (2015). Taut mooring system design and analysis of octagon FDPSO. Ocean Engineering Equipment and Technology 2(3), 175-183. (in Chinese)

Wang, F., Y. K. Zhang, Y. Wang, Z. Y. Xu, Z. Y. Zhang, T. Ni, J. J. Zhuang, Y. Tu and B. Y. Qian (2013). Floating non-traditional manufacture of floating drilling storage and offloading units-study on modeling and optimization method for the underwater rotating technology. Marine structures 31, 15-23.

Wang, S. S., J. R. Zhao, B. Xie, M. Fan and X. C. Yu (2013). Global performance analysis for deep water octagon FDPSO. Ship & Ocean Engineering 43(3), 183-189. (in Chinese)

Wang, W. H., L. L. Wang, Y. Z. Du, Y. X. Yao and Y. Huang (2016). Numerical and experimental analysis on motion performance of new sandglass-type floating body in waves. Marine structures 46, 56-77.

Wei, Y. F., J. M. Yang, G. Chen and Z. Q. Hu (2014). Numerical and model research on the hydrodynamic performance of FDPSO with single point mooring system. Journal of Ship Mechanics 18(4), 395-405. (in Chinese)

Wei, Y. F., J. M. Yang, G. Chen and Z. Q. Hu (2012). Numerical and Model Test Study on the Hydrodynamic Performance of FDPSO with Spreading Mooring System. Journal of Ship Mechanics 16(6), 603-616. (in Chinese)

Wei, Y. F., J. M. Yang, G. Chen and Z. Q. Hu (2011). Research on the concept design for deep-water multi-column semi-submersible FDPSO. Ocean Engineering 29(1), 1-8. (in Chinese)

Yao, Y. X., W. H. Wang, Y. Huang and M. S. Ye (2016). Analysis on deepwater mooring system of sandglass-type FDPSO. Journal of Shanghai Jiaotong University 2016 31(1), 23-28.

Yu, C. F., Z. Q. Hu and J. Wang (2016). Numerical analysis of heave performance for deep water octagon FDPSO. China offshore platform 31(1), 23-28. (in Chinese)